Strain-displacement compatibility and restoration of the Chaînes Subalpines of the western Alps

J.-P. Gratier, G. Ménard and R. Arpin

Geological Society, London, Special Publications 1989; v. 45; p. 65-81
doi:10.1144/GSL.SP.1989.045.01.04

Strain-displacement compatibility and restoration of the Chaînes Subalpines of the western Alps

J.-P. Gratier, G. Ménard & R. Arpin

SUMMARY: Finite strain values and trajectories of the sedimentary cover of the French Chaînes Subalpines (Chartreuse, Vercors, Diois, Baronnies) with respect to the stable platform west of these regions were deduced from the strain measurements of a folded and faulted competent layer (Tithonian). The removal of this finite deformation was obtained by a finite element analysis (84 elements of initial size of about 15×15 km) and the finite displacement field of this cover was calculated. Assuming a stable margin (one fixed element, and one line with a constant direction during the progressive deformation) the displacement of the eastern, southern and western limits of the Chaînes Subalpines were estimated. A displacement towards the west, associated with a counter-clockwise rotation (15–20°) was found for the Miocene–Present basement thrust of the Belledonne massif. The presence of local heterogeneities (such as Jurassic normal faults) deflect the general E–W displacement along dextral NE–SW and N–S strike-slip faults and induce a displacement of the Chaînes Subalpines towards the southwest. The comparison of the restored depth of the Tithonian with its estimated initial depth reveals an excess of elevation of the Chaînes Subalpines with a maximum value (1000–1500 m) for the Diois–Vercors which might be associated with an external basement thrust under the Chaînes Subalpines.

When considering the deformation of the external zone of the western Alps, three domains may be schematically distinguished on an E–W section (Fig. 1a).

The western part may be considered as a stable margin. The sedimentary cover overlying the eastern continuation of the basement of the Massif Central is horizontal. The basement/cover interface is also nearly horizontal, affected only by normal and strike-slip faults. The latest marine sediment (Miocene) lies only a few hundred metres above the level of its deposition in the Rhône Valley and in the Bas–Dauphiné plain (Fig. 2).

Within the central part (Fig. 1a), in general called the Chaînes Subalpines, the basement/cover interface also remains nearly horizontal and also is affected only by normal and strike-slip faults. The sedimentary cover, however, is folded, with a large décollement at the basement/cover interface, with several thrust faults within this cover, and with a high elevation of Miocene sediments (up to 2000 m above sea level).

Finally, the eastern part is the mobile margin, with large thrust faults in the basement carrying the Belledonne and Pelvoux massifs westwards over the Chaînes Subalpines (Ménard 1979), and with the basement/cover interface as much as 3000 m above sea level.

The aim of this study is to estimate the displacement of the mobile margin (Chaînes Subalpines) with respect to the stable area to the W. On a section parallel to the orientation of the principal strain (Fig. 1b), it is simple to estimate the displacement of a mobile margin. Following Ramsay (1969, 1976) and Hossack (1978), the displacement is obtained by the integration of the strain values along the strain trajectories. When considering a competent layer that has been folded (and faulted) without any change of thickness (such as the Tithonian limestone of the Upper Jurassic sequence), the displacement of the mobile margin (relative to the stable margin) is simply the difference between initial and final length of this layer. The problems in estimating this strain for the western Alps are first, that a part of the deformation is accommodated by strike-slip faulting, and second, that the finite strain trajectories are not straight, but curved. This clearly appears on a structural map (Fig. 2); the orientation of the fold axes changes from NNE–SSW in the Chartreuse to N–S in the Vercors, and in the Diois and Baronnies there are at least two orientations of Alpine folds (Goguel 1947). To remove the strain from such a heterogeneously deformed region, is not simple. Following Schwerdtner (1977) and Cobbold (1979), however, the removal of the finite heterogeneous deformation using strain trajectories may be accomplished by dividing the whole domain into several elements, such that the deformation of each element can be considered as homogeneous and continuous.

From: COWARD, M. P., DIETRICH, D. & PARK, R. G. (eds), 1989, *Alpine Tectonics*, Geological Society Special Publication No. 45, pp. 65–81.

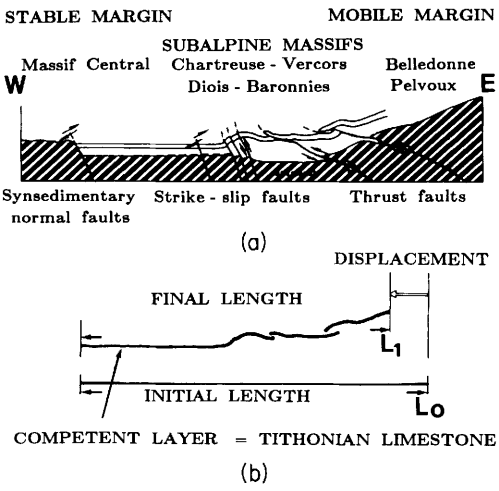

FIG. 1. (a) Schematic cross section through the Chaînes Subalpines from the stable margin (Massif Central) to the mobile margin (Belledonne–Pelvoux Massifs): hatched area = basement; arrows = movement on faults, either strike-slip or thrust. (b) Measurements of the displacement of the mobile margin, using the ratio of final length to initial length of a competent layer (folded and faulted without change of thickness), measured along a section parallel to the orientation of principal strain. The Upper Jurassic Tithonian limestone was used as a reference layer.

Method

The basis of the method used here was suggested by Schwerdtner (1977) and Cobbold (1979) and was clearly summarized by the latter author as follows: 'using the principal orientations, strain trajectories are constructed for the deformed state. The body is divided into finite elements bounded by these trajectories. Each element is then unstrained without changing its orientation or position. This process creates artificial voids and overlaps, which are minimized by imparting rigid translations and rotations to the elements. The result is the pattern of strain trajectories for the underformed state.' If we can choose both a line that did not undergo rotation during deformation and an element that did not undergo translation, then by comparing the strain trajectories before and after deformation, we can estimate the displacement of the mobile margins of the studied area with respect to this line and this element.

The first stage towards this aim was to determine the strain trajectories. This was done locally by measuring the horizontal strains (i.e. the ratio of the final, horizontal, length to the initial length of a folded competent layer) along three (or four) variously orientated cross sections across each area. (Fig. 3.) These regional strain measurements on cross sections allow us to calculate horizontal strain ellipses from place to place, with a slight overlap of the measured areas, for a greater accuracy of the strain orientations and magnitudes. To ensure a homogeneity of these strain values, the same value of 15 km was chosen as diameter of most unit circles (Fig. 3), in order to respect the assumptions of the method (i.e. homogeneous and continuous deformation of each element). This value is one order of magnitude greater than the displacement on the major thrust faults. For the eastern part of the Chartreuse, where large thrust displacement did occur, the diameter of the unit circle was 30 km.

The cross sections were drawn from 30 geological maps published at the scale of 1:50 000 (Bureau de Recherches Géologiques et Minières, France). For the Chartreuse and Vercors, recent seismic profiles were used to constrain the geometry of deep structures such as the décollement surfaces. The Tithonian limestone was chosen as the reference, or measured, layer, first, because it was folded without any change of thickness, and second, because it crops out throughout almost the entire Chaînes Subalpines. As often as possible the Urgonian limestone was also used to complete the estimation of the deformation from the Tithonian layer.

It was also necessary to take into account the effect of the strike-slip faults. This was accomplished for some regions, where the displacement along such faults is known from previous geological work (e.g. Goguel 1948, Gidon 1964, Arnaud 1981, François 1981), and a new strain ellipse was obtained as the product of the two different types of deformation. The deformation sequence is first folds and thrusts, then strike-slip faults.

With a knowledge of both the strain trajectories and the strain magnitude (treated as homogeneous and continuous within each measured area), the region can be divided into rectangular elements, with their sides parallel to the finite strain trajectories (Cobbold 1979). For a best possible adjustment of the elements restored to their initial unstrained state, the elements of the deformed state were drawn in order to have an initial size as close as possible to 15 km×15 km. Note, however, that if the grid in the strained state is chosen so that the sides of the elements are parallel to the finite strain trajectories, the shape and orientations of such elements in their initial unstrained state

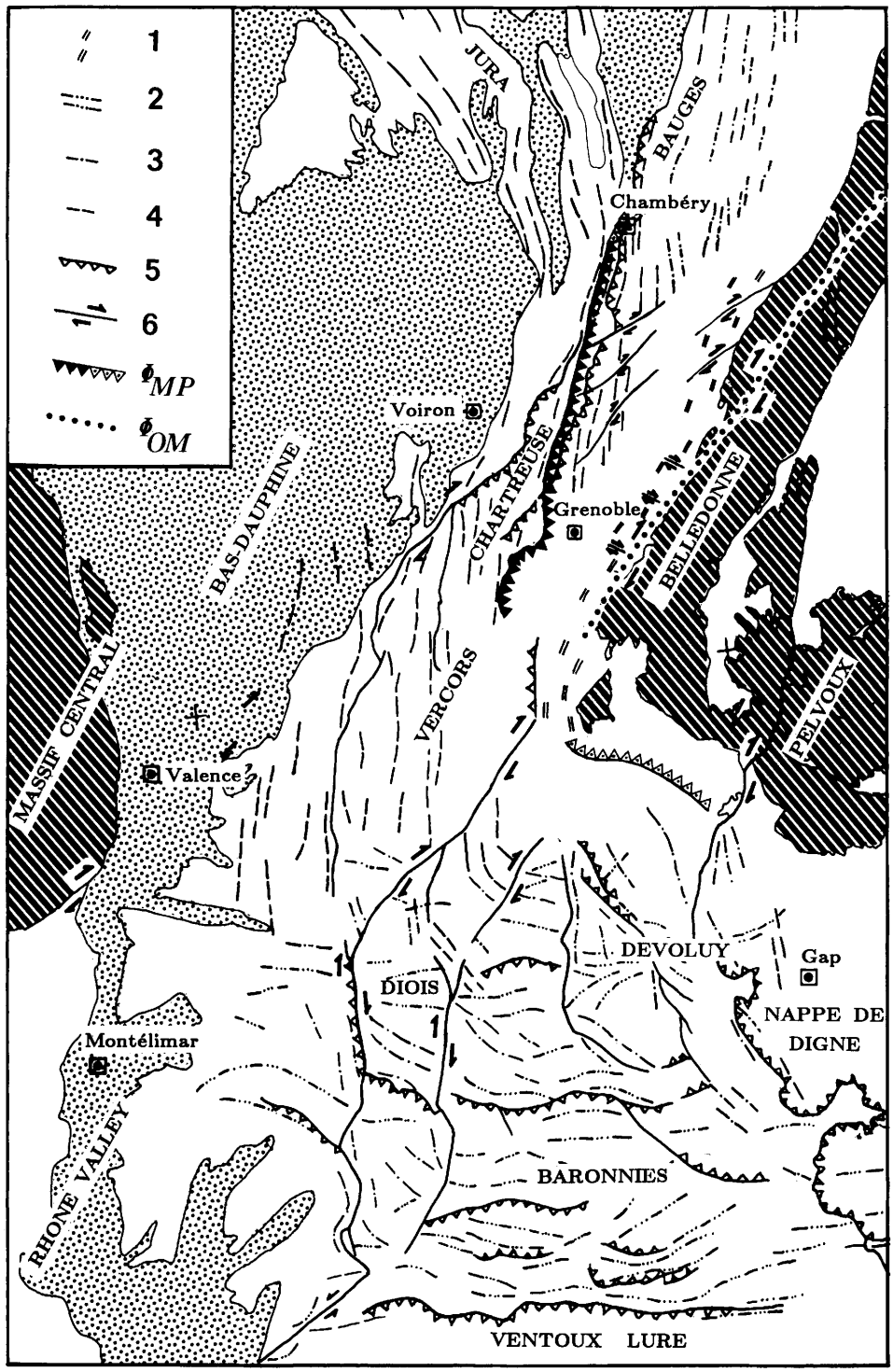

FIG. 2. Structural map of the Chaînes Subalpines showing the main structures of the region: 1 – spaced cleavage in the Jurassic slates of the cover of Belledonne; 2–3–4 – fold axes of different ages; 2 – Pyreneo–Provençal folds; 3 – Alpine folds (Oligo–Miocene); 4 – Alpine folds (Miocene–Present); 5 – main thrust faults; 6 – main strike-slip faults; hatched area – basement, shaded area – Tertiary; ϕ_{OM}–Oligo–Miocene basement thrust; ϕ_{MP}–Miocene–Present basement thrust (with black triangles = outcrop, with dotted triangles = presumed basement thrust concealed by the sedimentary cover).

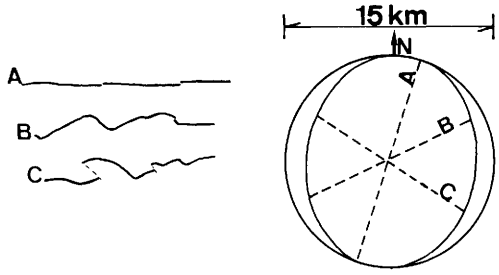

FIG. 3. Determination of strain trajectories and strain values by the measurement of the horizontal contraction (finite length L_1, initial length L_0) along three variously orientated cross sections A, B, C. The horizontal strain ellipses were calculated from place to place (with a slight overlap), for an initial length (L_0) of 15 km of the Tithonian limestone.

will not necessarily define a Cartesian grid (see Cobbold 1979). Therefore, since we cannot be sure that the initial strain trajectories conformed to a Cartesian grid (see Cobbold & Barbotin 1987), we cannot balance the magnitudes with the strain trajectories in order to have the same initial squares. To construct the deformed grid we simply used (independently) the strain trajectories deduced from the calculated strain ellipses (see above) and the magnitudes of strain measured along the sections parallel (or nearly parallel) to the principal strain directions. These continuous remeasurements of strain are necessary in order to avoid some gaps or overlaps of strain data along the strain trajectories.

An important source of error was the varying accuracy in the determination of the strain directions and magnitudes from place to place. In order to minimize these errors, the construction of the deformed grid was made by three successive stages, see Fig. 4(a):

(1) The first elements to be drawn were those with the most accurate strain magnitude data (regions with extensive outcrops of the Tithonian formation and with known displacements along the faults) and strain orientation data (those elements with only one principal direction of shortening).
(2) Second, we then drew the elements with accurate strain values (see above), but with relatively poor constraints on the orientations of principal strain (i.e. elements with either low strain values or with two principal orientations of shortening). For these elements, all of which lie between well constrained elements (Diois), the principal strain orientation was chosen to be compatible with that in the adjacent elements by assuming a smooth progressive variation in orientation as the strain values vary across the region. The problem of the western part of the studied area (Massif Central) will be discussed later (see discussion on the choice of the orientation of the undeformed grid). At this point, a first interesting observation is that it was possible to draw the best constrained elements in the deformed state such that the initial size of these elements was not far from a regular square of $(15\pm3)\times(15\pm3)$ km. This means that the strain trajectories transposed in the undeformed state were probably not very different from a Cartesian grid.
(3) To draw the elements with not very accurate strain data, complementary strain data were linearly interpolated from the adjacent elements in order to obtain an initial shape of these elements close to a square of $(15\pm1)\times(15\pm1)$ km. Of course, in the future this grid will have to be corrected after new strain measurements have been acquired for these elements. All the strain values used to construct the strain map are given in Table 1.

Another factor that can be useful for a tight control of the horizontal strain is the knowledge of the vertical strain. Both the depth of the décollement and the depth of the initial sedimentary reference layer (Tithonian limestone) are needed to estimate such vertical strains, when assuming constant volume in the deformation of each element. The depth of the décollement (which is often the basement/cover interface) is relatively well known in the western Alps, after the synthesis from seismic work and drill holes by Ménard (1979), and the results of new seismic profiles recently obtained through the Chartreuse (Thouvenot & Ménard 1989) and the Vercors (Arpin *et al.* 1988). On the contrary, an estimation of the depth of the Tithonian limestone before the sedimentary cover was folded is very difficult, because even over the region with horizontal sedimentary cover, the present depth of the top of the Tithonian formation varies from 0.5 km in the Bas–Dauphiné plain to 2.5 km in the Rhône valley (Fig. 2). In such areas it is clearly impossible to calculate the vertical strain, and therefore to balance these values with the horizontal strain. Nevertheless, using both the depth of the décollement and the horizontal strains (associated with folds and thrusts), it was possible to calculate the restored depth of the top of the Tithonian limestone (after the removal of the measured horizontal

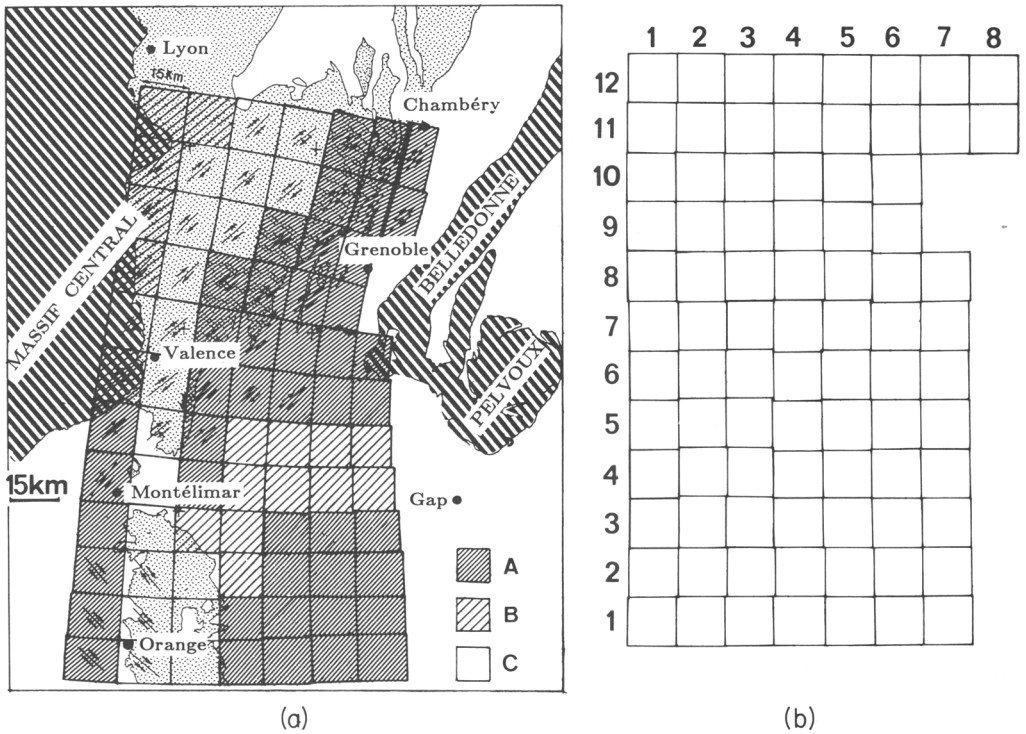

FIG. 4. (a) Deformation grid of the Chaînes Subalpines: using the strain values from measurements of the folded and faulted Tithonian formation (Fig. 3), the whole region was divided into 84 finite elements bounded by strain trajectories. The elements A, with both accurate estimation of strain values and principal directions, were drawn first. Then the elements B, also with good estimates of strain values but not with well constrained strain orientations, were drawn. Finally interpolations were made to draw the elements C, with few outcrops. The arrows within some elements indicate that strike-slip faults were taken into account to estimate the strain values for these elements. Hatched area: basement; shaded area: Tertiary. (b) Undeformed grid after the removal of the deformation of the elements and their adjustment. The figures of the rows and the columns give the reference of the elements in Table 1 where the strain values and strain orientation used for all the 84 elements are listed.

TABLE 1. *Strain values and principal horizontal strain orientations for the 84 elements of the finite deformation grid of the Chaînes Subalpines (Fig. 4a).*

1 – Reference number of the elements: horizontal row/vertical column of Fig. 4b
2 & 3 – Strain values associated with folds, thrusts and normal faults
4 & 5 – Strain values associated with strike-slip faults
6 & 7 – Finite strain values
8 & 9 – Finite strain directions

The elements 11/7–11/8 and 12/7–12/8 were grouped together in Fig. 4, since for these elements the displacement values on thrusts are larger than those for the other 80 elements.

strain). This depth must then be compared with the estimated initial minimum depth of the Tithonian formation necessary for the subsequent deposition of the entire marine sedimentary sequence after the Tithonian interval. The difference between the initial and the restored depths corresponds with the remainder of elevation after the strain has been removed, i.e. with the excess altitude of the Tithonian due to processes other than simple horizontal shortening of the cover above the basement (see discussion on vertical elevation).

1	2	3	4	5	6	7	8	9
1/1	1	.954	1.1	.909	1.1	.867	95	5
1/2	1	.971	1.1	.909	1.1	.883	91	1
1/3	1	.9	1	1	1	.9	88	178
1/4	.9	.933	1	1	.9	.933	88	178
1/5	1	.967	1	1	1	.950	88	178
1/6	1	.967	1	1	1	.967	88	178
1/7	1	.967	1	1	1	.967	88	178
2/1	1	.945	1.05	.952	1.05	.9	95	5
2/2	1	.911	1.05	.952	1.05	.867	90	0
2/3	.973	.850	1	1	.973	.850	87	177
2/4	.913	.863	1	1	.913	.863	87	177
2/5	.987	.820	1	1	.987	.820	87	177
2/6	.985	.757	1	1	.985	.757	87	177
2/7	1	.757	1	1	1	.757	87	177
3/1	1	.955	1.017	.983	1.017	.939	95	5
3/2	1	.955	1.017	.983	1.017	.939	90	0
3/3	.955	.980	1	1	.955	.980	89	179
3/4	.885	.922	1	1	.885	.922	89	179
3/5	.950	.894	1	1	.950	.894	88	178
3/6	.967	.9	1	1	.967	.9	88	178
3/7	.985	.937	1	1	.985	.937	85	175
4/1	1	.933	1	1	1	.933	95	5
4/2	1	.917	1	1	.990	.917	91	1
4/3	.937	.910	1	1	.937	.910	89	179
4/4	.885	.833	1	1	.885	.833	89	179
4/5	.934	.820	1	1	.934	.820	90	180
4/7	.917	.840	1	1	.917	.840	81	171
5/1	1	1	.968	1.033	.968	1.033	95	5
5/2	1	1	1	1	.985	.987	93	3
5/3	.935	.973	1	1	.935	.973	92	2
5/4	.867	.950	1	1	.867	.950	91	1
5/5	.906	.910	1	1	.906	.910	90	0
5/6	.870	.910	1	1	.870	.910	86	176
5/7	.877	.875	1	1	.877	.875	83	173
6/1	1	1	.968	1.033	.968	1.033	96	6
6/2	.983	1	.984	1.017	.967	1.017	95	5
6/3	.910	.917	.984	1.017	.895	.933	94	4
6/4	.867	.873	1	1	.867	.873	93	3
6/5	.910	.920	1	1	.910	.920	91	1
6/6	.885	.890	1	1	.885	.890	90	0
6/7	.833	.860	1	1	.833	.860	87	177
7/1	1	1	.923	1.083	.923	1.083	97	7
7/2	1	1	.923	1.083	.923	1.083	96	6
7/3	.924	1	.937	1.067	.866	1.067	96	6
7/4	.908	1	.937	1.067	.857	1.067	95	5
7/5	.913	1	.968	1.033	.884	1.033	94	4
7/6	.833	1	1	1	.833	1	93	3
7/7	.800	.933	1	1	.800	.933	90	0
8/1	1	1	.896	1.117	.896	1.117	97	7
8/2	1	1	.909	1.1	.909	1.1	97	7
8/3	.920	1	.937	1.067	.862	1.067	97	7
8/4	.850	1	.952	1.050	.809	1.050	97	7
8/5	.887	1	1	1	.887	1	97	7
8/6	.783	.967	1	1	.783	.967	96	6
8/7	.750	.950	1	1	.750	.950	92	2
9/1	1	1	.909	1.1	.909	1.13	97	7
9/2	1	1	.909	1.1	.909	1.1	98	8
9/3	1	1	.923	1.083	.923	1.083	99	9
9/4	.880	1	.923	1.083	.812	1.083	100	10
9/5	.887	1	.968	1.033	.859	1.033	102	12
9/6	.727	.933	1	1	.727	.933	102	12
10/1	1	1	.937	1.067	.937	1.067	97	7
10/2	1	1	.923	1.083	.923	1.083	98	8
10/3	1	1	.923	1.083	.923	1.083	100	10
10/4	.94	1	.937	1.067	.881	1.067	101	11
10/5	.87	1	.952	1.050	.829	1.050	103	13
10/6	.727	.983	1	1	.727	.983	104	14
11/1	1	1	.984	1.017	.984	1.017	96	6
11/2	1	1	.984	1.017	.984	1.017	96	6
11/3	1	1	.968	1.033	.968	1.033	98	8
11/4	1	1	.937	1.067	.937	1.067	100	10
11/5	.930	1	.909	1.1	.845	1.1	103	13
11/6	.75	1	.883	1.13	.662	1.13	105	15
11/7-8	.4	1	.870	1.15	.348	1.15	100	10
12/1	1	1	1	1	1	1	95	5
12/2	1	1	1	1	1	1	95	5
12/3	1	1	.968	1.033	.968	1.033	96	6
12/4	1	1	.937	1.067	.937	1.067	97	7
12/5	1	1	.896	1.117	.896	1.117	97	7
12/6	.8	1	.822	1.22	.658	1.22	98	8
12/7-8	.32	1	.789	1.267	.252	1.267	100	10

TABLE 1. (*cont.*). *Elements of the finite deformation grid.*

Strain calculation from cross sections

The strain data used to estimate the horizontal strain ellipses were deduced from numerous cross sections through the folded and faulted sedimentary cover. The geological data were obtained from the published 1:50 000 geological maps. The data on the deep structures were deduced from the synthesis by Ménard (1979) for the basement/cover interface (Diois–Baronnies), and from new seismic profiles (Chartreuse and Vercors).

A seismic profile from the Bauges to the Chartreuse (Thouvenot & Ménard 1989) revealed two interesting types of deep structures (Fig. 5, section 12a). The basement/cover interface was obtained both under the Chartreuse (parautochthonous and autochthonous basement) and under the Liassic cover of the Belledonne massif (overriding basement). A second interface within the sedimentary cover at a shallow depth (2–3 km) was also found to underlie the major part of the Chartreuse. This latter interface was interpreted as the top of a competent layer, and because no thick limestone layer is known to exist below the Tithonian limestone in the sedimentary sequence, this interface was considered to be the top of an autochthonous domain overlain by an allochthonous domain. After discussion (Mugnier *et al.* 1987), the interface was interpreted to represent the top of the Urgonian limestone instead of the Tithonian. With these geological and geophysical data, several balanced cross sections, which may be restored to their initial state, were drawn (Fig. 5, sections 6 to 12) (see Arpin *et al.* 1988 and Thouvenot & Ménard 1989).

The thrust sequence through the Chartreuse implies firstly the development of a large thrust (ϕ_1 = dashed line, Fig. 5) and secondly a later folding of this thrust associated with a décollement parallel to the Jurassic black shale (ϕ_2 = dotted line, Fig. 5). The ϕ_1 thrust surface is always complex with two levels of décollement (on an horizontal deep thrust surface within the crust, and along the Jurassic black shale) related to two ramps. During this thrust sequence the basement reached the top of the more external ramp, but did not climb over it (see sections 6 to 12, Fig. 5). The ϕ_2 thrusts occurred afterwards

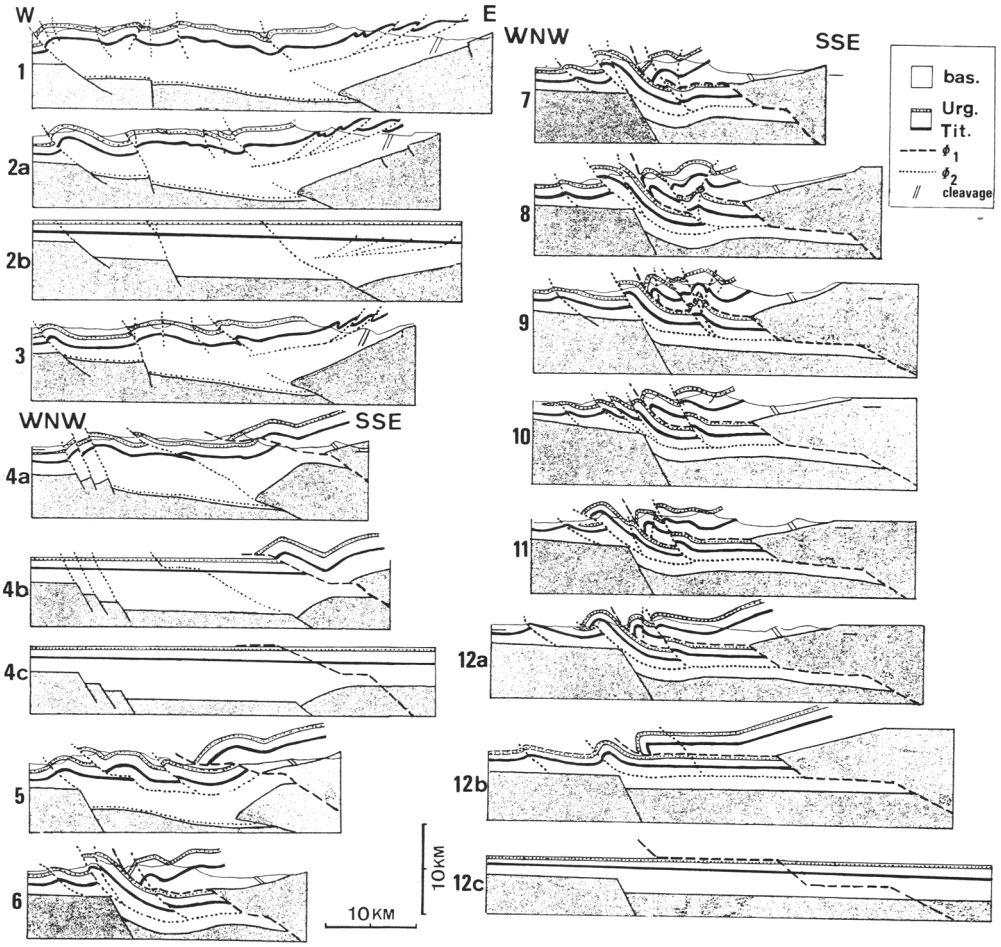

FIG. 5. Balanced cross sections through the Chartreuse and Vercors (after Arpin *et al.* 1988). Locations of sections are on Fig. 7. The restored state is given for three sections (2, 4, 12) with an intermediate stage between initial and finite deformation for sections 4 and 12. The geological surface data were obtained from the 1:50 000 published geological maps, from an unpublished 1:100 000 geological map of the Vercors (Arnaud 1981), and from local outcrop studies. The data on deep structures were deduced from seismic profiles (Arpin *et al.* 1988, Thouvenot & Ménard 1989). Shaded area: basement; the dotted double line is the Urgonian limestone (mid-Cretaceous formation); the thick line is the Tithonian limestone (Upper Jurassic); two types of thrust faults were distinguished: ϕ_1 = dashed line, ϕ_2 = dotted line.

because probably less work is needed to create new external thrust faults, parallel to the Jurassic black shales, than to cause large internal deformation of the basement by climbing over the second ramp. Note that the ϕ_2 surface may also be parallel to the basement/cover interface of the most external domain (see sections 6 to 12 in Fig. 5), where, because of the effect of normal faults, the depth of the basement/cover interface is almost the same as the Jurassic black shales under Chartreuse.

The ϕ_1 thrust can be followed up to the north of the Vercors (sections 4 and 5, Fig. 5, with an outcrop of the ϕ_1 surface on section 4a), but with a drastic decrease of the amount of the displacement towards the west. Consequently, towards the south of section 3 (Fig. 5), the geometry of the thrusts becomes different. The décollement surface is always found along the basement/cover interface. This discontinuity is deduced from seismic profiles, using explosions from working quarries near Grenoble (Arpin

et al. 1988). Other structures appear from section 3 towards the south (sections 1, 2, 3 in Fig. 5); back thrusts developed above the overriding basement and partially accommodated the horizontal E–W shortening of the cover, south of the termination of the ϕ_1 thrust.

The cross sections through the Diois and Baronnies cannot be balanced because both principal horizontal strains indicate shortening. These sections were simply drawn using the widespread outcrops of Tithonian limestone, which is never very far from the topographic surface, and is well mapped on the 1:50000 geological maps (Fig. 6).

In two regions there are no outcrops of the Tithonian limestone. In one region data from gravity studies reveal en échelon N–S folds along a NE–SW strike-slip fault (eastern limit of the Bas–Dauphiné plain, Orgeval & Rumeau 1955, Gamond & Odonne 1984). In the other region (Rhône valley), interpolations were made from adjacent regions (see method section).

Near the eastern limit of the Chartreuse, but east of the measured sections, a spaced cleavage affects the Jurassic slates of the Belledonne cover. Strain trajectories can be drawn assuming that this cleavage defines the X–Y strain plane (Ramsay 1967), (Fig. 2). A progressive change is observed in the orientation of the strain trajectories from west of Chartreuse (N10) to the western limit of Belledonne (N20–30), and will be discussed below.

Strain removal, displacement field

Strain removal and finite total displacement field

The first step was to remove the deformation in each element, then the elements in their initial shapes were displaced and rotated by hand in order to minimize the voids and the overlaps between neighbouring elements. The discrepancies between adjacent elements were distributed over the whole region by adjusting the lengths of the columns and of the rows in order to have the boundaries of the region as smooth as possible (Fig. 4b). The undeformed grid is not very different from a Cartesian grid, as anticipated previously when considering the small curvatures of the strain trajectories and the low finite strain gradient.

The next step was to choose the orientation of the Cartesian grid, superposed on the undeformed grid, in order to calculate first the transformation of the grid and then the displacement of the mobile margin. No sufficiently reliable data are available to infer the rigid rotation of a deformed region (see also Percevault & Cobbold 1982). Consequently, we used the following approach. As noted above, the continuation of the Massif Central (the Bas–Dauphiné Plain) acts as a rigid indentor, in front of which the folded sedimentary cover is heterogeneously deformed with a more or less symmetrical curvature of the strain trajectories between the Jura and the Vercors–Chartreuse Chaînes (Fig. 2). We chose the bisector of the triangular indentor as an unrotated line, in order to allow minor symmetrical shear zones on both the NE–SW (dextral) and on the NW–SE (sinistral) strike-slip faults along the limits of the indentor.

When points of the initial Cartesian grid are linked with those of the deformed grid, a schematic view of the relative finite displacement reveals a motion of the cover of the southern mobile zone towards the N and NW and a motion of the eastern mobile zone towards the W and SW (Fig. 8). Of course, this is not the true displacement path of the cover since several successive stages of deformation, with different orientations, occurred in the region. In order to discuss the displacement fields associated with each of these successive stages, the tectonic history and the major structural features of the Subalpine massifs must be considered.

Tectonic history and structural features of the Chaînes Subalpines

A simplified tectonic history of the Chaînes Subalpines may be summarized from the work of Goguel (1947), Flandrin (1966), Vialon (1974), Arnaud (1981), Gidon (1982), Tricart (1984) and Lemoine (1984) as follows.

Continental rifting of the European margin occurred during the deposition of the Lias–Dogger and is always associated with the tilting of large blocks bounded by variously orientated normal faults. These faults are often inherited from preceding structural events (i.e. the Massif Central structures). Within the area studied, synsedimentary normal faults were commonly reactivated as strike-slip or thrust faults (Fig. 2). At least four orientations of such normal faults have been revealed by stratigraphic studies: NE–SW faults (along the eastern limit of the Massif Central and Bas–Dauphiné Plain); N–S faults (through the Diois–Baronnies); E–W faults (between the Ventoux and the Baronnies); and NW–SE faults (along the south-west limit of the Belledonne–Pelvoux massifs). The development of these normal

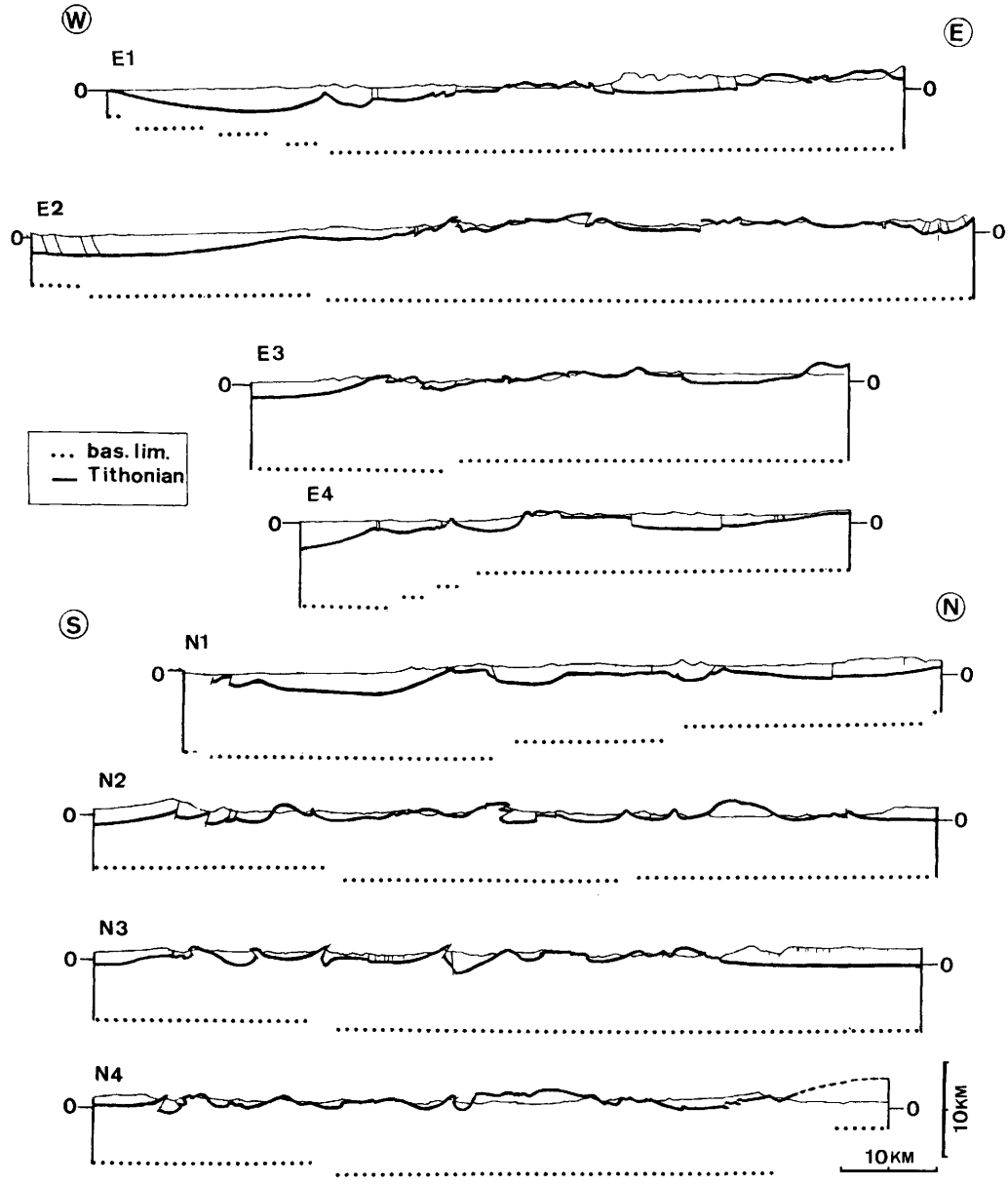

FIG. 6. Cross sections through the Diois and Baronnies (after Jouve, 1985). Locations of sections are on Fig. 7. The surface data were obtained from the 1:50 000 geological map, and the data on the basement/cover interface are from Ménard (1979). Dotted line: basement/cover interface; thick line: Tithonian limestone (Upper Jurassic).

faults implies extension with all horizontal orientations, but the E–W trending normal faults are rather localized in the southern part of the studied area. Nevertheless, the choice of the Tithonian limestone as reference layer allows us to assume that the effect of the Lias–Dogger horizontal extension was not registered by the strain measurements of the Tithonian limestone, because these phases of horizontal extension probably had ceased by the end of the Jurassic period. Nevertheless we shall see that these normal faults acted as heterogeneities and geometric discontinuities during the Alpine contraction (see discussion section).

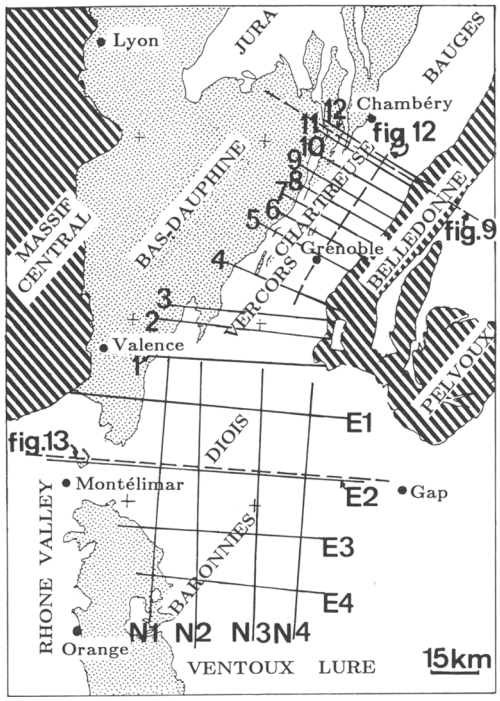

FIG. 7. Map showing locations of cross sections shown in Figs 5, 6, 9, 12 and 13a (1 to 12 on Fig. 5, E1 to E4 and N1 to N4 on Fig. 6). Dashed area: basement; shaded area: Tertiary.

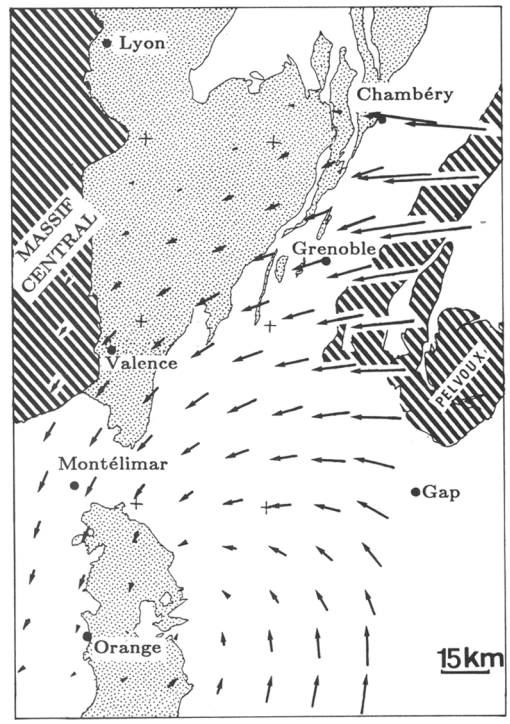

FIG. 8. Finite total displacement field: shortest path from points on a Cartesian grid (superposed on the undeformed grid) to points on a finite deformation grid (see Fig. 4b and a). Dashed area: basement; shaded area: Tertiary.

The contraction phases, which occurred afterwards, may be schematically divided into two stages: Pyreneo–Provençal and Alpine (Fig. 2).

The Pyreneo–Provençal stage began with the development of the pre-Senonian E–W folds of the Diois–Baronnies linked to a NNE displacement of the limit of the southern mobile belt. The N–S contraction increases from west to east and is associated with sinistral NE–SW strike-slip faults (Arnaud 1973). These E–W folds were locally amplified during the Cenozoic part of the Pyreneo–Provençal stage (up to the Miocene for the Ventoux thrust).

The Alpine stage, in the Chaînes Subalpines, probably began during the Oligocene, and is linked to the first large basement thrusts of the Belledonne massif, now sealed between the internal and the external domains of Belledonne (ϕ_{OM}, Figs 2 and 9). We named this first basement thrust 'Oligo-Miocene' (ϕ_{OM}). Its effect, largely seen in the deformation of the Bauges (Doudoux *et al.* 1982), decreases from north to south. Movement on this fault is probably not very important in the Chartreuse and is almost nil in the Vercors, but the spaced cleavage of the Jurassic slates between Chartreuse and Belledonne may be associated with this thrust. The major E–W contraction of the Chartreuse–Vercors–Diois instead was associated with the development of a second more external basement thrust of the Belledonne massif, active from the Miocene to the present, here named Miocene–Present thrust (ϕ_{MP}). The N–S fold axes (often along pre-existing N–S normal faults), the dextral strike-slip movement along these faults, and an amplification of the Pyreneo–Provençal E–W folds may be associated with this Alpine stage (Diois–Baronnies), see Goguel (1963). Other basement thrusts have been anticipated in the western part of the main ϕ_{MP} basement thrust (Fig. 5), but following Ménard & Thouvenot (1984), these thrusts do not continue below a shallow décollement surface within the basement (Fig. 9). Finally, the effect of the basement thrusts of the Pelvoux massif toward the west (Fig. 2) must also be taken into account to explain the E–W contraction of the Diois–Baronnies (see discussion section).

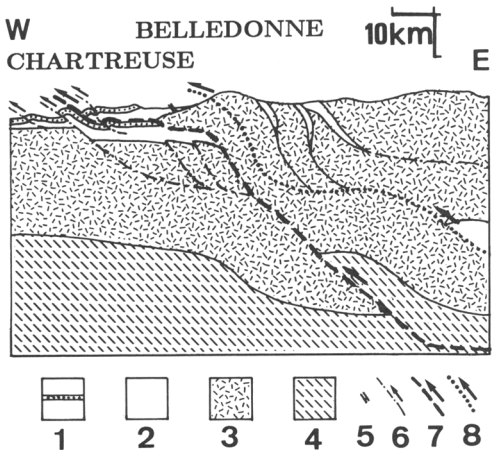

FIG. 9. Balanced crustal cross section, from Ménard & Thouvenot (1984), showing the two main basement thrusts: Miocene–Present external thrust dashed line (7) = ϕ_{MP}; and Oligo–Miocene thrust, dotted line (8) = ϕ_{OM}; (6) other thrusts. The spaced cleavage of the Jurassic slates of the Belledonne cover (5) may be related to the ϕ_{OM} thrust. (3) and (4), upper and lower crust; (2), sedimentary cover; (1), Tithonian to Urgonian formations.

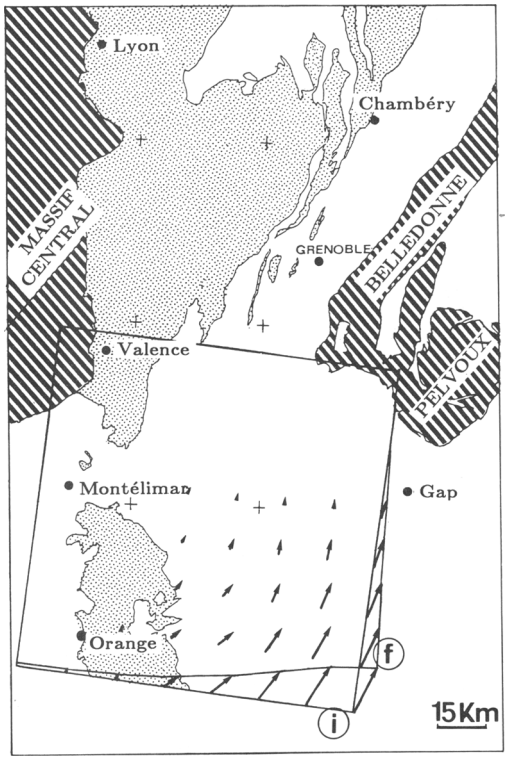

FIG. 10. Finite displacement field associated with the Pyreneo–Provençal stage of deformation: initial (i) to final (f) state; dashed area basement; shaded area Tertiary.

Finite Pyreneo–Provençal displacement field

The discrimination between the Pyreneo–Provençal and Alpine deformation is not easy, but an attempt was made to distinguish the displacement pattern for each stage. Following the geological evidence given above, a Pyreneo–Provençal deformation model was drawn using the N–S contraction values measured within the Diois–Baronnies, associated with the displacement towards the NNE. The amount of the NNE displacement decreases from east to west (from 15 to 1 km) and from S to N (up to an underformed domain near the limit between Vercors and Diois). The displacements associated with the E–W horizontal extension were taken to vary from zero along the northern limit of Diois to a maximum value of 5 km along the southern limit of Baronnies. The region with extension is limited by the Rhône valley (using the whole measured finite E–W horizontal extension, Table 1), and no significant extension is seen along the E–W Diois–Baronnies folds. The resulting displacement pattern is given in Fig. 10. The progressive changes of both the amount and the orientation of the displacements were derived from the measured strains and assumed boundary conditions.

Finite Alpine displacement field

The difference between the total finite deformation and the Pyreneo–Provençal deformation gives the Alpine deformation, with a simpler pattern of displacement (Fig. 11) than that of the total finite displacement (Fig. 8). The main characteristics of this Alpine displacement are that the limit of the eastern mobile zone is carried towards the W. The progressive increase of this E–W cover displacement, from the S (5 km) to the N (30 km) implies a counter-clockwise rotation of this eastern limit of the Tithonian outrops of about 15–20° (Fig. 11). The presence of a NE–SW stable domain along the western limit of the Vercors–Chartreuse massifs induces a lateral expulsion of the sedimentary cover towards the southwest, with a general counter-clockwise rotation of the Chaînes Subalpines.

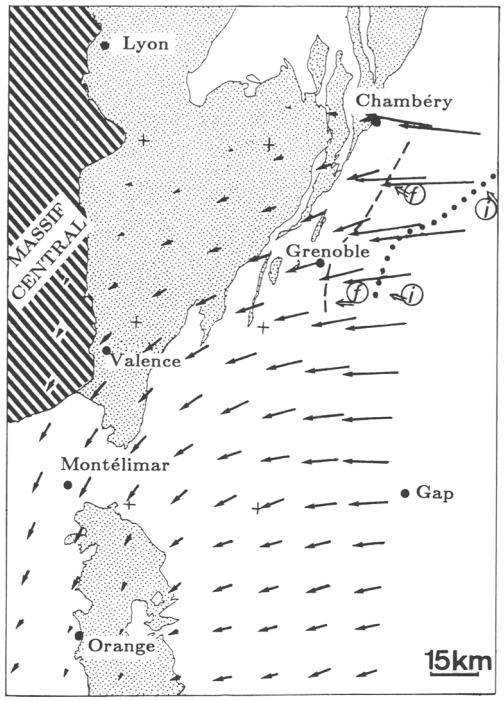

FIG. 11. Finite Alpine displacement field deduced from the difference between the total displacement field (Fig. 8) and the Pyreneo–Provençal stage (Fig. 10). The present western limit of the hanging wall ramp of the Miocene–Present thrust of the Belledonne Massif is drawn as a dashed line, its initial state (after the removal of the Alpine deformation) is drawn as a dotted line. The double arrows indicate the direction of displacement deduced from measurements of magnetism of samples in their present position (f) and in their reconstructed initial position (before the Miocene–Present thrust) (i); dashed area, basement; shaded area, Tertiary.

(a) Displacements of the mobile zone along the western stable limit

Along the NE–SW trending limit of the Vercors–Chartreuse (probably a Jurassic system of normal faults) the displacement of the sedimentary cover is clearly associated with a dextral strike-slip movement on these NE–SW trending faults, and also with the development of N–S trending folds along pre-existing N–S normal faults (with reversal in the sense of slip on these faults, see Gillcrist *et al.* 1987, and Fig. 5). Through the Diois–Baronnies, the displacement towards the SW is mainly deflected along two major N–S trending dextral strike-slip faults (Fig. 2), again Jurassic normal faults reactivated with a component of thrust displacement. The geological observations bear no clear evidence for relating these N–S trending faults with the faults on the NE–SW limit of the Vercors–Chartreuse. The Alpine dextral displacement, at the north termination of the N–S faults of the Diois instead is partitioned into several divergent branches (N–S to NE–SW dextral strike-slip, see Fig. 2). The general counter-clockwise rotation of the Chaînes Subalpines is limited in the W by two parallel fault systems that curve from NE–SW to N–S: one along the eastern part of the Massif Central–Bas Dauphiné, and the other along the western limit of the Diois–Baronnies. Such a system of lateral expulsion, associated with large amounts of counter-clockwise rotation, with curved X–Y finite strain trajectories within this deformed domain and limited by NE–SW dextral strike-slip faults, has already been described within the Bourg d'Oisans basins by Gratier & Vialon (1980). The same geometry of lateral termination of a mountain belt is also proposed by Molnar & Lyon-Caen (1989).

The horizontal displacement of the sedimentary cover, which progressively decreases from the mobile (eastern) to the stable (western) limit, has to be related to the mechanical and geometrical properties of the décollement zone. In the particular case of the Diois–Baronnies, the pre-existing Cretaceous E–W folds induced an anisotropic behavior of the cover, with a relative weakness along the N–S direction that facilitated the counter-clockwise rotation of these regions.

(b) Displacement along the eastern mobile limit: Belledonne massif

Another problem is the relation between the displacement of the cover and that of the basement, especially near the eastern mobile limit of the Chaînes Subalpines. The evidence of two successive basement thrusts in the Belledonne Massif (Fig. 9) requires an estimation of the part of the cover displacement associated with each of these basement thrusts. For example, the strains registered by the spaced cleavage of the Jurassic slates (east of the eastern limit of the shortening measurements of the Tithonian, Fig. 2), must not be used to estimate the displacement of the basement associated with the Miocene–Present basement thrust, because this cleavage is clearly above the ϕ_{MP} basement thrust (see Fig. 9). Probably, either this part of the cover was passively transported (piggy-back) by the Miocene–Present thrust with the cleavage being associated with the Oligo–Miocene basement thrust, or this cleavage developed during gravity sliding movements (in this case

associated with the tilting of the basement acquired during the Miocene–Present thrust). In contrast, the deformation registered by the Tithonian folds and faults through the Chartreuse–Vercors may be associated entirely with the displacement of the Miocene–Present basement (including the back-thrusts between Vercors and Belledonne). This displacement may be visualized by drawing the western limit of the basement hanging wall ramp and by calculating the initial position of this line using the strain data of the Tithonian layer. This was done in Fig. 11, where a 15–20° counter-clockwise rotation was associated with the westwards displacement of the basement, together with an horizontal extension parallel to the Belledonne Massif (less than 20%). As in the Chartreuse, this NNE–SSW extension of the Belledonne Massif was probably accommodated by strike-slip faulting: dextral ENE–SSW faults and WNW–ESE sinistral faults (clearly visible all along the Belledonne Massif, Gratier *et al.* 1973). A part of the internal deformation of the Belledonne basement may also be associated with the Alpine deformation. The deformation history observed through the Belledonne schists closely matches the Alpine deformation history of the sedimentary cover of the Belledonne and Pelvoux Massifs (Gratier & Vialon 1980): asymmetric folds with slaty cleavage, reorientation of the fold axes from the Y into the X direction with increasing strain, crenulation cleavage, and Riedel faults. All these structures indicate thrust movement towards the west, on shear planes dipping towards the east.

(c) Displacement along the eastern mobile limit: Belledonne–Pelvoux transition

The problem of the SW end of the Belledonne basement thrust will now be discussed. The ϕ_{MP} basement thrust (Fig. 11) shows a decrease of displacement from N of Chartreuse (30 km) to the mid Vercors (15 km), but most of this decrease is acquired S of the Chartreuse and N of the Vercors. On a schematic NNE–SSW section (Fig. 12), it clearly appears that the decrease of the thrust displacement is associated with a lateral ramp. More exactly, the depth of the flat level of the autochthonous Urgonian unit (acting as the décollement interface) rapidly increases from its value N of Vercors to that S of Chartreuse, just at the latitude of Grenoble. It may be noted that after the removal of the Belledonne thrust the southwest limit of Belledonne is just the SE prolongation of the NW–SW part of the Isère valley (from Grenoble to Voiron, Fig. 2). This NW–SE trending limit could represent an old fault re-actived during the Alpine deformation firstly as sinistral strike-slip fault (to accommodate the different amounts of westward displacement between Chartreuse and Vercors), and secondly as fault with vertical movement (Fig. 12). When taking into account the geometric compatibility of the deformation of the cover associated with the counter-clockwise rotation (Fig. 4), these vertical movements must be associated with a thrust fault near Grenoble and a normal fault near Voiron. An explanation for the abnormal vertical elevation of the Vercors massif will be discussed later (see discussion on the partitioned vertical elevation): the NW–SE part of the Isère valley could be a lateral ramp of a recent external basement thrust under the Baronnies, Diois and Vercors (see Fig. 13a).

Finally, even if the ϕ_{MP} Belledonne thrust displacement decreases from north to south, there remain 15 km of horizontal E–W displacement SW of the end of the Belledonne Massif. From this zone to the actual end of the region with E–W contraction (south of the Baronnies) other basement thrusts through the Pelvoux Massif have to exist (Fig. 2). Understanding

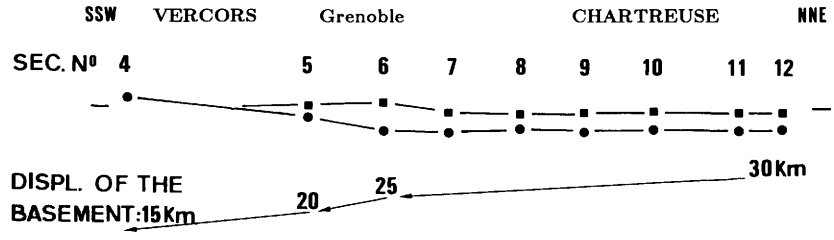

FIG. 12. Schematic longitudinal cross sections along the Chartreuse–Vercors, showing elevations of the autochthonous Urgonian limestone (black points), estimated along a flat level of décollement (ϕ_1), and showing the variation in elevation of the allochthonous Tithonian limestone (black squares). The position of this longitudinal cross section is indicated on Fig. 7. The values of the westwards displacement of the basement are given below the section (15–30 km).

this clearly requires complementary strain measurements through the Devoluy and the nappe de Digne structure. In any case, it is possible that the basement of the Pelvoux massif was thrust towards the SW, laterally bounded by NE–SW dextral strike-slip faults (Gidon *et al.* 1976). The early Oligo–Miocene thrust of Belledonne was reactived as a strike-slip fault during this Pelvoux thrusting movement (Ménard & Fréchet 1989), (Fig. 2). As this Belledonne strike-slip fault may continue through the Vercors–Diois as a NE–SW strike-slip fault (Fig. 2), the same movement is observed for the basement and the cover: a lateral expulsion towards the SW limited by strike-slip faults, and associated with a counter-clockwise rotation.

(d) Relation with the development of the western Alpine arc

The strain removal based on the Tithonian limestone indicates a progressive change of the orientation of the displacement from N95 (north of the Chartreuse) to N80 (mid-Vercors). The same change in orientation was recently revealed by the study of the magnetic anisotropy of cleaved Jurassic slates sampled between Chartreuse–Vercors and Belledonne Massif (Lamarche & Rochette 1987, Aubourg 1987): the displacement direction varies from N125 at the latitude of the north of Chartreuse to N90 at the mid-Vercors latitude (double arrows on Fig. 11). As noted above, the cleavage in the Jurassic slates was probably not directly associated with the Miocene–Present basement thrust. If this cleavage is associated with the Oligo–Miocene basement thrust (see Fig. 9), the removal of the Miocene–Present deformation implies a variation of the Oligo–Miocene thrust orientation from N145 (Chartreuse) to N110 (Vercors). A contemporaneous NNE–SSW extension parallel to the Belledonne Massif is registered by numerous tension gashes (up to 10% of horizontal extension, Gratier 1984) in the Jurassic slates of the Belledonne cover, and probably also by strike-slip faults (see above). These directions are relatively approximate depending on the mechanism of rotation of the basement (rigid rotation and/or internal distortion). In all cases, the same counter-clockwise movement could be associated with the westwards motion of the two successive basement thrusts of the Belledonne Massif. The same evolution is also suggested by Vialon *et al.* (this volume), in the context of the movement of the entire western Alps. A counter-clockwise rotation of the Belledonne Massif associated with its westwards movement is linked to the general displacement of the Apulian indentor (African Plate) towards the N and the NW.

Limits and accuracy of the results

As noted above, the method used to remove the finite deformation of a sedimentary cover is based upon several assumptions. Different assumptions could lead to a different displacement field. The strain map (Fig. 4) is clearly a first attempt to take into account all the geometric features of a deformed area, but, of course, corrected strain values may always be introduced. Here, the various possibilities of error in the strain data will not be discussed for each element, we discuss only the possible errors associated with the orientation of the initial Cartesian grid (see method section). If the same fixed element (e.g. 12/1, the nearest to Lyon in Fig. 4) is considered, but with a slightly different orientation (±5°) of the initial grid, the following differences in the displacement field are introduced.

With a different orientation of 5° clockwise of the initial grid, the estimated direction of the displacement towards the west for the eastern limit varies from N115 (north of the Chartreuse) to N135 (Vercors–Diois limit), with an associated change in the displacement of the eastern limit from 30 to 10 km. A N135 direction of displacement along the southwestern limit of the Pelvoux Massif seems unrealistic since most measured orientations of contraction through this region (Goguel 1963, Gidon 1982) are approximately NE–SW (from NNE–SSW to ENE–WSW). For the western limit, a displacement towards the east would be required by strain compatibility. This similarly unrealistic displacement can be reduced by changing the interpolated strain values along the Rhône valley (see Fig. 4), with a progressive increase southward of the E–W horizontal extension from Lyon (nil) to more than 15 km for the southern limit, and of course yet more towards the Mediterranean. This also seems to be incompatible with the geological evidence.

With a different orientation of 5° counter-clockwise, the displacement direction of the eastern limit varies from N75 (north of Chartreuse) to N70 (Vercors–Diois limit), the displacement values varying from 30 km (Chartreuse) up to 25 km (Vercors). In this case, the N75 direction of finite displacement is clearly difficult to accept for the Chartreuse with its NNE–SSW trending folds, and also N75 trending strike-slip faults (see Fig. 2). For the western limit, a large

displacement toward the SW, with an increasing value from Lyon (nil) to for example 15 km (Montelimar), and yet more towards the S, is also difficult to accept (but it is not as unrealistic as are the directions of displacement).

These two examples show the limits and also the accuracy of the results. Taking into account all the geological constraints, it is possible to estimate that the directions of the finite displacement may vary by ±10°, and the displacement values by ±10–20%, due to the discrepancy in the orientation of the initial grid.

Partitioned vertical elevations

It remains now to discuss the vertical elevations associated with the measured horizontal contraction. As noted previously (see method section), it is not possible to balance the horizontal and the vertical strain since the initial level of the reference layer (Tithonian), just before the Alpine contraction, varies greatly from place to place. A restored elevation of the Tithonian was calculated, using the amount of horizontal contraction for groups of four elements, and assuming constant volume during the deformation of the cover above the décollement surface, which commonly lies at the basement/cover interface. The depth of this décollement is known from seismic profiles (Thouvenot & Ménard 1989, Arpin *et al.* 1988). The great size of the analysed blocks (30×30×10 km) allows us to assume constant volume deformation. This restored elevation was then matched with the estimated initial elevation of the Tithonian limestone (that is the minimum depth of the Tithonian limestone necessary to allow the deposition of the marine sedimentary sequence above this Tithonian limestone, Fig. 13a). The difference between the two values gives an excess of elevation of the Tithonian limestone due to processes other than the folding and thrusting of the cover above the basement. This excess altitude was plotted on a map (Fig. 13b). A maximum excess elevation of 1000 to 1500 m clearly appears for the south Vercors, the northern and eastern Diois, and the eastern Baronnies. These values decrease towards the west to less than 500 m in the Bas–Dauphiné plain and in the Rhône valley (southwards of a prolongation of the Diois). Applying the same model used to explain the elevation of the Belledonne basement (basement involved thrust faulting), the excess altitude of the Chaînes Subalpines might be due to the development of a new external basement thrust (see Fig. 13a), with a blind thrust now just below the Rhône valley. A very small displacement (of some kilometres, according to Molnar & Lyon-Caen 1988), is sufficient to explain the calculated excess altitude if the thrust affects the whole thickness of the crust as do the Belledonne and Pelvoux thrusts.

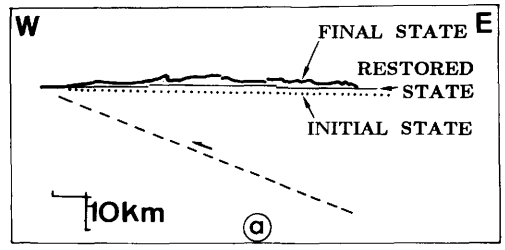

FIG. 13. (a) Comparison between the present elevation of the Tithonian limestone, the elevation after the removal of the finite deformation, and the elevation necessary for the deposition of the marine sequence covering the Tithonian. An external basement thrust (dashed line) may explain the excess of elevation of the Tithonian. The location of the section is shown on Fig. 7.

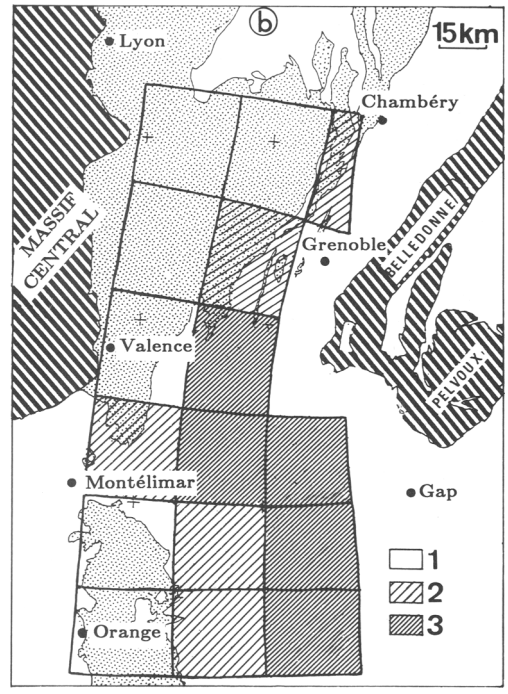

FIG. 13. (b) Distribution of the excess elevation of the Tithonian s.l. through the Chaînes Subalpines. Dashed area, basement; shaded area, Tertiary; excess altitude from 1000 to 1500 m (3), from 500 to 1000 m (2), and from 0 to 500 m (1).

Conclusions

In a large heterogeneously deformed region, the finite displacement field may be deduced from an analysis of regional finite strains by dividing the whole region into several homogeneous finite elements and by integrating these strain values along the strain trajectories.

From strain localised in the folds and thrusts of the Tithonian limestone of the Chaînes Subalpines, associated with the Miocene–Present basement thrust of the Belledonne Massif, the Alpine finite displacement directions and amounts indicate a westwards movement of the eastern limit of the Chaînes Subalpines, and an associated counter-clockwise rotation of 15–20° of this limit, with respect to the underformed stable part of the Massif Central.

NE–SW to N–S trending Jurassic normal faults along the stable margin (Massif Central) deflect the westwards displacement of the Chaînes Subalpines toward the SW and locally towards the S. A general counter-clockwise rotation of the Chaînes Subalpines is observed, limited along the stable margin by dextral strike-slip faults which reactivated the pre-existing Jurassic normal faults.

After the removal of the folding and thrusting of the Tithonian limestone, the restored depth of this layer was calculated (using the décollement surface deduced from seismic data) and matched with the estimated initial depth of the Tithonian (depth of the marine deposition of the overlying sedimentary sequence). An excess of altitude was found (up to 1500 m) especially for the southern Vercors, the Diois and the eastern Baronnies, which could be due to a present external basement thrust under the Chaînes Subalpines associated with the lateral expulsion of these regions.

Such a system of Alpine lateral expulsion, associated with large amounts of rotation, with arcuate X–Y finite strain trajectories within this deformed domain, and limited by curved strike-slip faults along the stable margin, is one of the possible geometries of lateral termination of a mountain belt.

Finally, this work is only a first attempt to take into account all the geological and geophysical data that constrain the amounts and orientations of deformation in a heterogeneously deformed region. The finite deformation grid may always be corrected, as soon as new data are acquired. In a general way this method of restoring a sedimentary cover which is heterogeneously deformed between stable and mobile margins could be applied to other regions, to study the geometry and the displacement field of lateral termination of mountain belts.

ACKNOWLEDGEMENTS: We thank D. Dietrich, P. Molnar and the anonymous reviewers for their careful revision of this paper.

References

ARNAUD, H. 1973. Mise en évidence d'un important décalage anténiocène de sens senestre le long de la faille de Presles (Vercors occidental). *Comptes-Rendus de l'Académie des Sciences Paris*, **276**, 2245–8.

—— 1981. De la plate-forme urgonienne au bassin vocontien: le Barremo–Bédoulien des Alpes occidentales entre Isère et Büech. *Géologie Alpine*, **12**. Unpublished Thèse d'Etat, Grenoble.

ARPIN, R., GRATIER, J. P. & THOUVENOT, F. 1988. Chevauchements en Vercors et Chartreuse déduits de l'équilibrage de données géologiques et géophysiques. *Comptes-Rendus de l'Académie des Sciences Paris*, **307**, 1779–89.

AUBOURG, C. 1987. *Etude de la fabrique magnétique des Terres Noires subalpines*. Unpublished Diplôme d'Etudes Approfondies, Université de Grenoble.

BUREAU DE RECHERCHES GEOLOGIQUES ET MINIÈRES: 1:50000 geological maps of La Tour du Pin, Chambéry, Voiron, Montmélian, Serrière, Beaurepaire, Grenoble, Domène, Romans, Vif, Vizille, Valence, Charpey, La Chapelle en Vercors, La Mure, Crest, Die, Mens, St Bonnet, Dieulefit, Luc en Diois, Gap, Valreas, Nyons, Serres, Orange, Sederon, Avignon, Carpentras, Sault. Orléans, France.

COBBOLD, P. R. 1979. Removal of finite deformation using strain trajectories. *Journal of Structural Geology*, **1**, 67–72.

—— & BARBOTIN, E. 1988. Kinematic significance of fanning strain trajectories. *Journal of Structural Geology*, **10**, 811–8.

DOUDOUX, B., MERCIER DE LEPINAY, B. & TSARDY, M. 1982. Une interprétation nouvelle de la structure des massifs subalpins savoyards (Alpes occidentales): nappes de charriage oligocène et déformation superposées. *Comptes-Rendus de l'Académie des Sciences Paris*, **295**, 63–8.

FLANDRIN, F. 1966. Sur l'âge des principaux traits structuraux du Diois et des Baronnies. *Bulletin de la Société Géologique de France*, **7**, **VIII**, 376–86.

FRANCOIS, D. 1981. L'étude des accidents méridiens de Saillans–Mérindol et de Die-la-Motte–Chalançon (Diois–Baronnies). Unpublished rapport, Institut Français du Pétrole.

GAMOND, J. F. & ODONNE, F. 1984. Critères d'identifi-

cation des plis induits par un décrochement profond: modélisation analogique et données de terrain. *Bulletin de la Société Géologique de France*, **7**, **XXVI**, 115–28.

GIDON, M. 1964. Nouvelle contribution à l'étude du massif de la Grande-Chartreuse et de ses relations avec les régions avoisinantes. *Travaux du Laboratoire de Géologie Alpine*, **40**, 187–205.

—— 1982. La reprise de failles anciennes par une tectonique compressive: Sa mise en évidence et son rôle dans les Chaînes Subalpines des Alpes occidentales. *Géologie Alpine*, **58**, 53–68.

——, PAIRIS, J. L. & APRAHANIAN, J. 1976. Le linéament d'Aspres-lès-Corps: sa signification dans le cadre de l'évolution structurale des Alpes occidentales externes. *Comptes-Rendus de l'Académie des Sciences Paris*, **282**, 271–4.

GILLCRIST, R., COWARD, M. & MUGNIER, J. L. 1987. Structural inversion and its controls: examples from the Alpine foreland and the French Alps. *Geodinamica Acta*, **1**, 5–34.

GOGUEL, J. 1947. Recherches sur la tectonique des Chaînes Subalpines entre le Ventoux et le Vercors. *Bulletin de la Service Carte Géologique de la France*, **223, XLV**, 533–78.

—— 1948. Sur le rôle des failles de décrochement en Chartreuse. *Bulletin de la Société Géologique de France*, **5, XVII**, 227–35.

—— 1963. L'interprétation de l'arc des Alpes occidentales. *Bulletin de la Société Géologique de la France*, **7, V**, 20–33.

GRATIER, J. P. 1984. *La déformation des roches par dissolution-cristallisation: aspects naturels et expérimentaux de ce fluage avec transfert de matière dans la croûte supérieure.* Unpublished Thèse d'Etat, Grenoble.

——, LEJEUNE, B. & VERGNE, J. L. 1973. *Etude des déformations de la couverture et des bordures sédimentaires des massifs cristallins externes de Belledonne, des Grandes Rousses et du Pelvoux.* Unpublished Thèse 3ème cycle, Université de Grenoble.

—— & VIALON, P. 1980. Deformation pattern in a heterogeneous material: folded and cleaved sedimentary cover immediately overlying a crystalline basement (Oisans, French Alpes). *Tectonophysics*, **65**, 151–80.

HOSSACK, J. R. 1978. The correction of stratigraphic sections for tectonic finite strain in the Bygdin area, Norway. *Journal of the Geological Society of London*, **135**, 229–241.

JOUVE, J. F. 1985. *Analyse quantitative de bassins plissés et reconstitution de leur état initial: exemple du Diois–Baronnies.* Unpublished, Diplôme d'Etudes Approfondies, Université de Grenoble.

LAMARCHE, G. & Rochette, P. 1987. Microstructural analysis and origin of lineation in the magnetic fabric of Alpine slates. *Tectonophysics*, **139**, 285–93.

LEMOINE, M. 1984. La masse occidentale de la Tethys ligure et les Alpes occidentales. *In*: BOILLOT, G. (ed). *Les marges continentales en mer et à terre autour de la France*, Masson, 155–248.

MENARD, G. 1979. *Relation entre structures profondes et structures superficielles dans le Sud-Est de la France. Essai d'utilisation de données géophysiques.* Unpublished Thèse 3ème cycle, Grenoble.

—— & THOUVENOT, F. 1984. Coupes équilibrées crustales: méthodologie et applications aux Alpes occidentales. *Geodinamica Acta*, **1**, 35–45.

—— & FRECHET, J. 1988. Mécanismes au foyer de séismes des Alpes occidentales et modèle de déformation actuelle de la Chaîne. *Earth and Planetary Sciences Letters*, in press.

MOLNAR, P. & LYON-CAEN, H. 1988. Some simple physical aspects of the support, structure and evolution of Mountain belts. *Geological Society of America*, Special publication no. 218.

—— & —— 1989. Fault plane solution of earthquakes and active tectonics of the northern and eastern parts of the Tibetan Plateau. *Philosophical Transaction of the Royal Society of London*, in press.

MUGNIER, J. L., ARPIN, R. & THOUVENOT, F. 1987. La construction de coupes équilibrées: méthodes et applications au nord du massif subalpin de la Chartreuse. *Geodinamica Acta*, **1**, 125–37.

ORGEVAL, M. & RUMEAU, J. L. 1955. Préreconnaissance du bassin de Valence. Bureau de Recherche du Pétrole. *Collection Institut Français du Pétrole*, **5054**.

PERCEVAULT, M. N. & COBBOLD, P. R. 1982. Mathematical removal of regional ductile strains in central Brittany: evidence for wrench tectonics. *Tectonophysics*, **82**, 317–28.

RAMSAY, J. G. 1967. *Folding and Fracturing of Rocks.* McGraw-Hill, New York.

—— 1969. The measurement of strain and displacement in orogenic belts. *In*: KENT, P. E., SATTERTHWAITE, G. E. & SPENCER, A. M. (eds). *Time and Place in Orogeny*, 43–79.

—— 1976. Displacement and strain. *Philosophical Transactions of the Royal Society*, **A283**, 3–25.

SCHWERDTNER, W. M. 1977. Geometric interpretation of regional strain analysis. *Tectonophysics*, **39**, 515–531.

THOUVENOT, F. & MENARD, G. 1989. Allochthony of the Chartreuse Subalpine massif: seismic constraints. *Journal of Structural Geology*, in press.

TRICART, P. 1984. From passive margin to continental collision: a tectonic scenario for the western Alps. *American Journal of Science*, **284**, 97–120.

VIALON, P. 1974. Les déformations synchisteuses superposées en Dauphiné. Leur place dans la collision des éléments du socle préalpin. *Bulletin Suisse de Minéralogie et Pétrographie*, **54**, 553–690.

J.-P. GRATIER, G. MÉNARD & R. APRIN, LGIT Observatoire de l'Université de Grenoble, IRIGM BP 68 38402 Saint-Martin d'Hères Cedex, France.